

Increasing the refractive index of materials via nanolamination: a-IGZO/TiO₂ nanolaminates

David Caffrey,^{1,2,3,*} Emma Norton,^{1,2} Cormac Ó. Coileáin,^{1,2} Christopher M. Smith,¹
Igor V. Shvets,^{1,2,3} and Karsten Fleischer^{1,2,3}

¹*School of Physics, Trinity College Dublin, Dublin 2, Ireland*

²*Centre for Research on Adaptive Nanostructures and Nanodevices (CRANN), Trinity College Dublin, Dublin 2, Ireland*

³*Advanced Materials Bio-Engineering Research Centre (AMBER), Trinity College Dublin, Dublin 2, Ireland*



(Received 6 June 2018; published 11 September 2018)

We investigate nanolamination as a means of increasing the refractive index of materials, with a focus on [amorphous InGaZnO (a-IGZO)/TiO₂]_i nanolaminates as composite transparent conducting oxides with a tunable index. We demonstrate that by periodic layering with TiO₂ the refractive index of a-IGZO can be increased by up to $\Delta n \approx 0.39$ while the carrier mobility and conductivity retain 70% of their original values. This is shown to be a result of the alignment of the conduction bands of a-IGZO and TiO₂. We also use optical modeling to verify the integral refractive index behavior of the nanolaminates and outline its range of applicability.

DOI: [10.1103/PhysRevMaterials.2.096002](https://doi.org/10.1103/PhysRevMaterials.2.096002)

I. INTRODUCTION

Transparent conducting oxides (TCOs) are vital components of modern technology, being essential in a variety of fields including display technology [1], thin-film transistors [2,3], thin film solar cells [4–7], and organic light-emitting diodes [8,9]. The performance of optoelectronic devices, based on current TCOs, can suffer due to internal interface reflections, which arise from the mismatch in the refractive index between successive layers. The simplest method to reduce such reflections is the inclusion of an internal antireflective layer with a refractive index which has a value between the two adjacent materials [10]. This process is trivial in cases such as the glass/air interface where a matching material can be applied easily [11]. Unfortunately, the same concept is complicated in the case of interfaces between the TCO and the active light-emitting diode or absorber material because the matching layer in this case must also be both transparent and conductive to maintain device function. This is compounded by the comparatively narrow available range of refractive indices ($n \approx 1.9$ – 2.2) for commercial TCOs such as ZnO:Al, indium tin oxide (ITO), and amorphous InGaZnO (a-IGZO) [12–14]. A generic method of altering the refractive index of any given TCO is thus advantageous. A variety of techniques have previously been demonstrated including interface roughening, nanoparticle inclusion, and cation substitution [11,15,16]. However, such methodologies are not universally applicable as they can have an unwanted effect on the crystallographic, electrical, or optical properties of the overall device.

In recent years a variety of studies have been published demonstrating the efficacy of high-periodicity multilayer structures in tuning material properties. Such structures, often referred to as superlattices or nanolaminates, typically

consist of two materials layered at periodicities of <10 nm with the intent of creating a composite material with new or enhanced properties. To date such periodic multilayers have been used to control ferromagnetic properties [17], oxidation states [18], environmental stability [19,20], resistive switching [21], superconductivity [22], dielectric properties [23], optical properties [24], photoluminescence [25,26], magnetoelectric effects [27], thermoelectric effects [28–31], and gas barriers [20]. Previously we reported on a methodology for tuning the refractive index of materials via the use of [TCO/dielectric]_i superlattice/nanolaminate structures [32]. These laminate TCOs enabled conservation of the conductivity and mobility of the component TCO material while reducing the composite refractive index of the structure in the visible range. This is achieved by the periodic inclusion of nanoscale layers (1–10 nm) of a material of differing refractive index. If the individual layer thickness (d) is significantly below the wavelength (λ) of the incident light ($\lambda \gg d$), the light will interact with the nanolaminate as though it has a laminate refractive index, n_L , which is equal to the integral of the individual refractive indices over the whole structure [33,34]. This $\lambda \gg d$ condition is often referred to as the thin-film limit, the long-wavelength limit, or the quasistatic regime.

In this work we expand upon the tuning of n_L by demonstrating how such a methodology can be applied to increase the refractive index of a TCO material by the selection of an appropriate tuning layer. We show that the conductivity of the nanolaminates can be maintained at close to the original bulk TCO value by choosing a material with a small conduction band offset with respect to the base TCO. We demonstrate this by synthesizing and characterizing [a-IGZO/TiO₂]_i nanolaminates which show a tunable refractive index increase combined with a high conservation ($>70\%$) of conductivity and carrier mobility of the stack. TiO₂ was selected due to its optical transparency and high refractive index [35] in conjunction with its favorable electrical properties [36,37] and conduction band alignment to a-IGZO.

*dcaffrey@tcd.ie

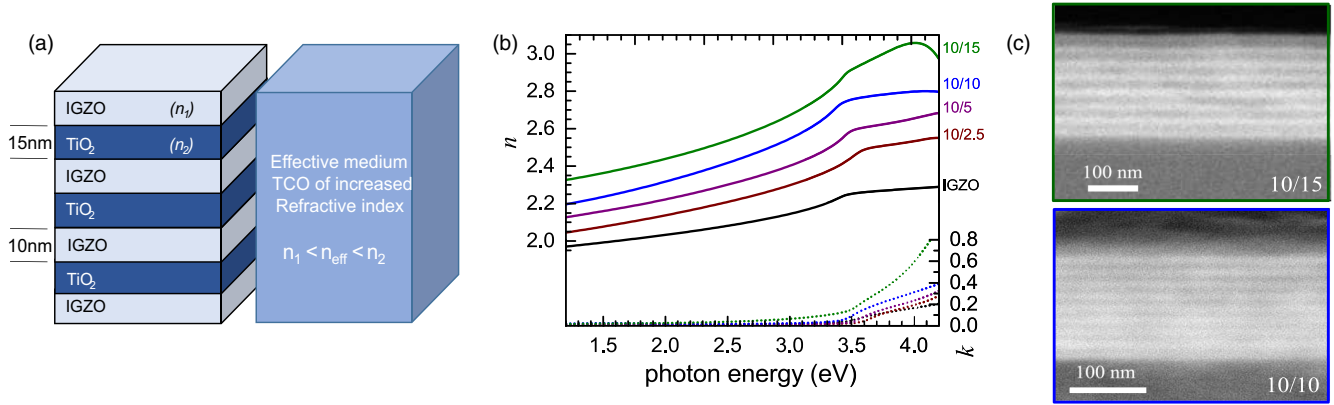


FIG. 1. (a) Schematic diagram of the structure of the nanolaminates and their response to visible range light. Middle panel: Real (n) and imaginary (k) parts of the complex refractive index of the $[a\text{-IGZO}/\text{TiO}_2]_i$ nanolaminates. (b) Backscatter detector SEM image of a $[10\text{ nm}/15\text{ nm}]_i$ nanolaminate. (c) Secondary electron image of a $[10\text{ nm}/10\text{ nm}]_i$ nanolaminate.

II. RESULTS AND DISCUSSION

All samples were deposited using radio-frequency (RF) magnetron sputtering. The details of the system and deposition methodology employed to form the superlattices are described elsewhere [32]. Samples were deposited on glass substrates using 2-in ceramic targets $[a\text{-IGZO} (1:1:1 \text{ In:Ga:Zn}) \text{ and } \text{TiO}_2]$. The substrate temperature during deposition was 450°C for all samples. Individual a-IGZO layers were kept at 10-nm thickness for all nanolaminates while the TiO_2 thickness was varied from 2–15 nm to control the refractive index of the TCO. The total nanolaminate thickness was kept at 190–200 nm. Nanolaminates were always terminated with an a-IGZO layer for consistent contacting during electrical measurements. The structure of the samples was confirmed by cross-sectional scanning electron microscopy (SEM) and x-ray reflection (see Fig. 1 and Supplemental Material [38], respectively). All films were post-annealed in N_2 at 320°C with *in situ* monitoring of the conductivity to further improve the electrical properties. Hall measurements were made with the four-point Van der Pauw method using silver wire electrical contacts and a 0.8-T magnet. Sheet resistance and Hall resistance were measured simultaneously to remove any effects of thermal drift.

X-ray diffraction (Bruker D8 Advanced) of the nanolaminates confirmed their amorphous nature, meaning that effects on the refractive index due to any change in crystallography of the TiO_2 [35,39,40] can be neglected. Ellipsometric measurements on all samples were performed using a Sopra GESP5 ellipsometer at incidence angles of 62° , 65° , and 68° . Fitting of the ellipsometry data, and the determination of the dielectric function of the stack thereby, was performed using a Jones-transfer-matrix-based calculation. The thickness of the stacks was obtained externally via x-ray reflection and was not used as a fitting parameter. The dielectric function was fitted with a dispersion law composed of a three-dimensional critical point in combination with a Lorentzian oscillator in the UV to account for above band-gap absorption. With the inclusion of the TiO_2 layers a pair of additional low-intensity Lorentzian oscillators were required at 1.5 and 1.9 eV to account for additional absorption of the defective TiO_2 .

Refractive indices of the deposited a-IGZO films and $[a\text{-IGZO}/\text{TiO}_2]_i$ nanolaminates obtained are shown in Fig. 1. As expected, the refractive index of the laminate TCO is found to increase with the increase in the thickness of the included TiO_2 layers. By inclusion of periodic 15-nm layers of TiO_2 the refractive index of the laminate TCO can be increased by $\Delta n \approx 0.39$ with respect to bulk a-IGZO. Considering the narrow band of refractive indices of many of the best-performing n -type TCOs such as ITO [41], ZnO:Al [16], fluorine-doped tin oxide [42], indium zinc oxide [43], and IGZO [32], the demonstrated capacity to change the refractive index by such a margin could enable improvements not readily achievable otherwise. In addition to the altered real refractive index, the extinction coefficient (k) shows a small increase in the 1.5–2 eV range upon increase of the TiO_2 thickness due to the defective nature of the amorphous TiO_2 . However, the effect of this on the transmission is minimal, with a relative change of only $\sim 1\text{--}2\%$ in the visible range observed in the $[10/15]_i$ (196-nm) nanolaminate relative to the 110-nm full a-IGZO reference sample. Another effect of the inclusion of the TiO_2 layers is a red-shift of the onset of absorption due to the lower band gap of the TiO_2 relative to the a-IGZO reference sample. Despite this the films are still highly transparent in the visible range with the onset of absorption remaining above 3 eV. Figure 2 shows estimated examples of the optical improvements in devices possible using refractive index tuning nanolaminates. These are calculated via Fresnel equations in a transfer matrix method using the dielectric functions determined in this work. Figure 2(a) compares the reflectance of an air/ $[(a\text{-IGZO})_{10\text{ nm}}/(\text{TiO}_2)_{10\text{ nm}}]_{15}$ (50 nm) interface vs that of an air/a-IGZO interface. For this calculation the media are assumed to be bulk (effectively infinite thickness) to aid in comparison by removing the effects of thin-film interference. As expected an increase in reflection is observed in the nanolaminate case due to the increased refractive index mismatch between the material and air. However, a reduction in reflectance, and thus an increase in transmission, can be observed when the nanolaminate is placed as an antireflective layer between a low- and a high-index medium as discussed above. This is shown in Fig. 2(b), which indicates the degree of improvement that can be achieved by the use of a

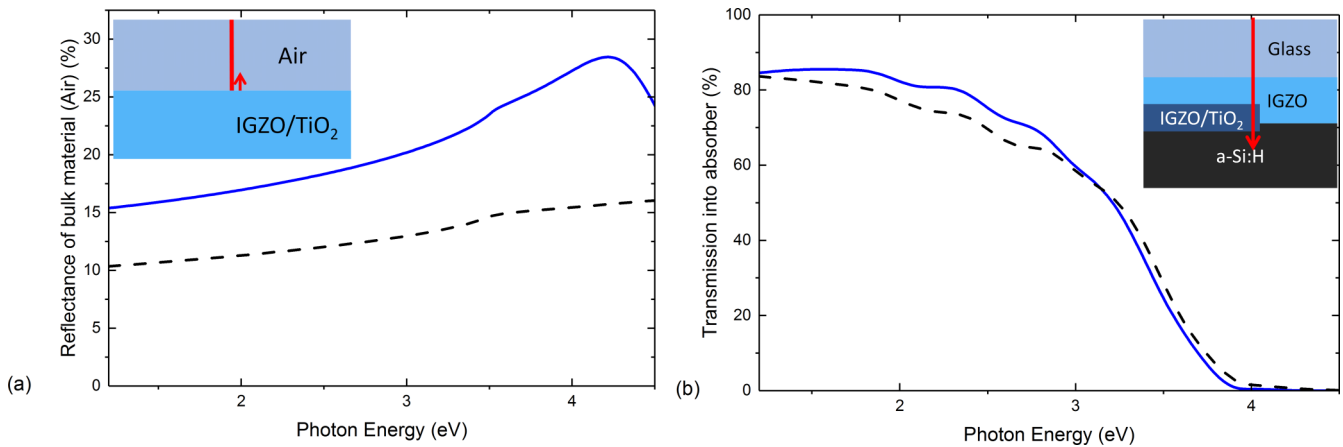


FIG. 2. (a) Reflectance of the air/bulk [a-IGZO/TiO₂]_i (—) interface compared to that of the air/bulk a-IGZO (---) calculated via transfer matrix using the dielectric functions of the individual media. An increase of the reflectance is observed due to the increase of the refractive index of [a-IGZO/TiO₂]_i. (b) Comparison of the calculated total transmission of light through to the absorber in a pair of simple demonstrative solar cells with (—) and without (---) an [a-IGZO/TiO₂]_i antireflective layer. Calculations performed using a glass/a-IGZO(500 nm)/a-Si:H solar cell and a glass/a-IGZO(450 nm)/[a-IGZO]_{10 nm}/(TiO₂)_{10 nm}]₁₅ (50 nm)/a-Si:H solar cell. The red arrow indicates the path of the light, with the point indicating where the interaction is calculated. All spectra were calculated for normal incidence of the light. Placing an [a-IGZO/TiO₂]_i nanolaminate at the TCO/absorber interface reduces the reflection at that point, leading to an improvement of the transmission to the absorber region across the visible spectrum.

nanolaminate in such a role in a demonstrator cell structure. The transmission to the absorber is calculated for two device architectures, one with an antireflective nanolaminate (glass/a-IGZO(450 nm)/[(a-IGZO)_{10 nm}/(TiO₂)_{10 nm}]₁₅ (50 nm)/a-Si:H) vs one without (glass/a-IGZO (500 nm)/a-Si:H). A wide spectral improvement of transmission to the a-Si:H absorber (5% at 2 eV) can be observed by the use of the nanolaminate at the TCO/absorber interface due to the reduction of the index mismatch. We wish to highlight that the calculated a-IGZO-based cell structure is only meant as a demonstration of achievable optical improvements and is not meant to represent an electronically effective cell. However, we feel that this illustrates the promise of these tuning layers. Beyond the benefits of the optical changes, the most important factor of this technique is how the electrical properties of the nanolaminates are maintained even when layers of 15 nm of TiO₂ are utilized and the n_L is increased by ≈ 0.39 .

Figure 3 shows the conductivity σ and the Hall mobility μ_H as a function of the refractive index (at 2 eV) (see also Table I) alongside results reported previously for the [a-IGZO/SiO_x]_i nanolaminates [32]. Clearly the electron mobility and the conductivity are well preserved, with a [10/10 nm]_i nanolaminate exhibiting a change of $\Delta n \approx 0.25$ while retaining 75% of the conductivity of unaltered a-IGZO and another [10/15]_i nanolaminate showing similar conservation with a change of $\Delta n \approx 0.4$ while maintaining 71% of the initial TCO conductivity. The conductivity of the films is found to have a nonlinear relation to film thickness; there is an initial decrease with the inclusion of the 2.5-nm-thick TiO₂ layers. The inclusion of thicker TiO₂ layers, up to 10 nm, results in progressively smaller deviations from the original conductivity up to 10 nm, beyond which it slowly decreases. The initial decrease is likely a result of under-stoichiometric ultrathin TiO₂ similar to that observed in corresponding [a-IGZO/SiO₂]_i nanolaminates [32], although the scale of the effect is substantially smaller. Nonstoichiometric TiO₂ could

equally reduce the carrier concentration of the a-IGZO layers, affecting the conductivity of the films. As the stoichiometry recovers with increasing TiO₂ thickness the effect on subsequent a-IGZO layers is reduced. Alternatively, Ti doping has been previously shown to have a gettering effect on a-IGZO carriers [44]; thus Ti diffusion into the a-IGZO could also reduce the carrier concentration. However, as the effect seen here is only observed in those nanolaminates which have ultrathin TiO₂ dielectric spacers, oxygen vacancy diffusion is the more likely cause. To summarize, the results obtained for the [a-IGZO/TiO₂]_i nanolaminates show significant improvement relative to the [a-IGZO/SiO_x]_i nanolaminates where a change of $\Delta n \approx 0.2$ leads to a reduction to 33% of the original conductivity and mobility. In comparison the [a-IGZO/TiO₂]_i nanolaminates can be tuned by a range twice as large while maintaining a conductivity of $>70\%$ the original value. The origin of these improvements can be understood by examining the relative band alignment of the a-IGZO, TiO₂, and SiO₂ layers.

Previous work indicates that a-IGZO [45] and TiO₂ [46] possess a comparatively low conduction band offset with respect to each other. This would facilitate improvements in the overall electrical properties of the nanolaminates as the tunnel barrier between individual TCO layers is reduced or ideally carriers can directly be injected from the TCO into the dielectrics conduction band. However, the band alignment would need to be verified experimentally for the TiO₂ films grown here, as it has been previously demonstrated to vary depending on crystallographic orientations and structure as well as on intrinsic doping levels [47,48]. Similarly the In:Ga:Zn:O ratios of a-IGZO also affect its band structure.

We therefore combined x-ray photoelectron spectroscopy (XPS) valence band measurements of all materials used in the nanolaminates (a-IGZO, TiO₂, SiO₂) with measurements of the absorption coefficient [$\alpha = -\ln(T + R)/d$], using UV-visible spectrophotometry in transmission (T) and reflection

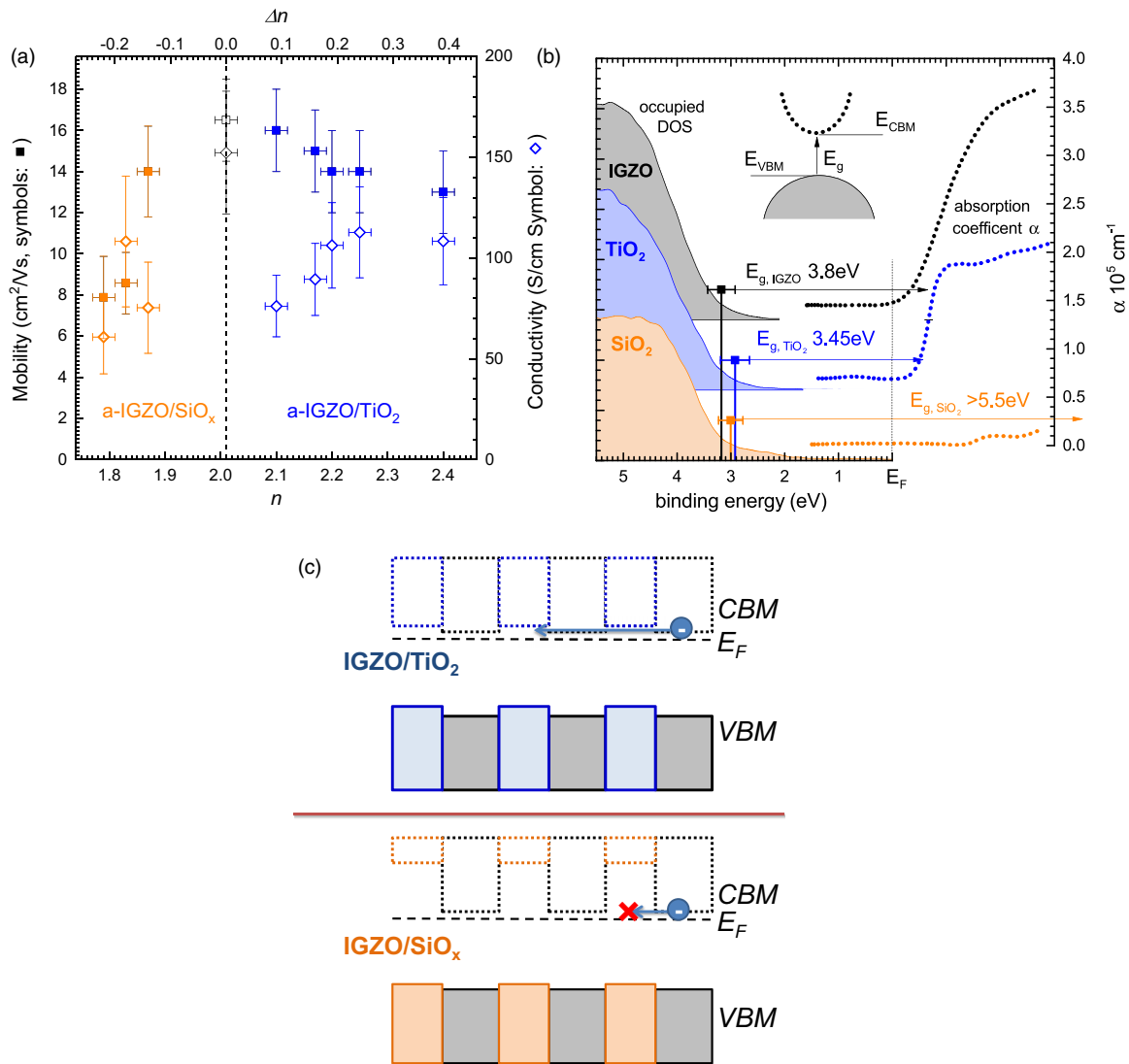


FIG. 3. (a) Mobility and conductivity of the nanolaminates as a function of the refractive index. Values for the refractive index are taken at $h\nu = 2$ eV ($\lambda = 620$ nm). On the bottom axis are the values of the refractive index for the nanolaminates and on the top axis are the changes in the refractive index relative to the value for the bulk sample. The electrical properties are found to be well conserved with the changing refractive index. The symbols are as follows: \square , bulk 110-nm a-IGZO; and \blacksquare , [a-IGZO/TiO₂]_{*i*} nanolaminates; \diamond , [a-IGZO/SiO_x]_{*i*} nanolaminates. The dashed line indicates the values for bulk a-IGZO. (b) Measured valence band spectra and absorption coefficients for bulklike films (~ 100 nm) of a-IGZO, TiO₂, and SiO₂ grown under conditions similar to those of the nanolaminates. To visualize the relative positions of the conduction bands between the materials, the energy scale of the absorption coefficient was aligned to the top of the valence band for each material. (c) Schematic illustration of the impact the band alignment has on electron transport through the dielectric interlayers. The top and bottom images illustrate [a-IGZO/TiO₂]_{*i*} and [a-IGZO/SiO_x]_{*i*}, respectively.

(*R*) in combination with the overall thickness (*d*). Films for absorption measurements were grown on sapphire samples to facilitate measurements at the onset of absorption in the UV spectral range, while films for the XPS measurements were grown on ITO-coated glass to minimize charging effects during the XPS measurements.

Figure 3 plots the two measurements on a joined energetic scale, allowing assessment of the conduction band offsets. The energy scale for each absorption measurement has been aligned to the valence band maximum as determined by XPS. While the latter is directly proportional to the density of states (DOS) of the filled valence band, the absorption data are proportional to the joined DOS of dipole allowed

transitions between filled and empty states and hence are not direct measurements of the conduction band DOS. However, a significant absorption indicates that there are empty states in that particular energy region. The measurements confirm that our a-IGZO films are highly *n*-doped, but not degenerate, while the TiO₂ films are natively *n*-type-doped, leading to a residual conductance of this particular dielectric. The small conduction band offset of 0.1–0.3 eV between a-IGZO and TiO₂ explains why the electrical properties of the [a-IGZO/TiO₂]_{*i*} nanolaminates outperform those of the [a-IGZO/SiO_x]_{*i*} nanolaminates. The same analysis shows SiO₂ to be insulating with a band gap outside our measurement range (>5.5 eV). However, XPS and the absorption

TABLE I. Measured geometry and total TCO ($d_{a\text{-IGZO}}$) and film thickness (d_{Total}) of the $[\text{a-IGZO}/\text{TiO}_2]_i$ nanolaminates deposited on glass. The measured sheet resistance R_s and the Hall mobility μ_H are also given.

Label	Nanolaminate geometry	$d_{\text{a-IGZO}}; d_{\text{Total}}$ (nm)	R_s (Ω/\square)	μ_H (cm^2/Vs)
	IGZO	110	597	16.5
10/2.5	$[(\text{IGZO})_{10\text{nm}}/(\text{TiO}_2)_{2.5\text{nm}}]_{15}$	160;198	660	16.0
10/5	$[(\text{IGZO})_{10\text{nm}}/(\text{TiO}_2)_{4.8\text{nm}}]_{12}$	130;188	581	15.0
10/7.5	$[(\text{IGZO})_{10\text{nm}}/(\text{TiO}_2)_{7.4\text{nm}}]_{11}$	120;201	451	14.0
10/10	$[(\text{IGZO})_{10\text{nm}}/(\text{TiO}_2)_{10\text{nm}}]_9$	100;190	450	14.0
10/15	$[(\text{IGZO})_{11\text{nm}}/(\text{TiO}_2)_{15.5\text{nm}}]_7$	88;196	471	13
	TiO ₂	100	>1 G	
	SiO ₂	100	>1 G	

measurements for SiO₂ show significant defect states that are likely to increase the tunneling probability and it is likely this is the origin of the observable conductivity of the $[\text{a-IGZO}/\text{SiO}_2]_i$ nanolaminates, despite the significant offset in their conduction bands. Thus we can link the improved properties of the $[\text{a-IGZO}/\text{TiO}_2]_i$ nanolaminates to better overlap in band position between the TCO and the refractive index tuning layers.

So far, we have demonstrated that by taking the band alignment of the materials into account, it is possible to construct refractive-index-altering nanolaminate structures without compromising their electrical properties. Due to its importance to this work, the method used for obtaining the refractive indices of the nanolaminates merits a more detailed discussion. In many cases the estimation and fitting of the dielectric function of an inhomogeneous medium is performed via theoretical effective medium approximation models. These models are based on the assumption or requirement of the $\lambda \gg d$ behavior and often approximate the inhomogeneity in some manner, most famously as randomly distributed spherical inclusions in the Maxwell-Garnett and Bruggeman approaches [49,50]. However, these models are typically based on the assumption that the inhomogeneity level is below the percolation threshold, the level at which the inhomogeneities are no longer randomly distributed and instead begin to cluster. Unfortunately the assumptions made in these models break down in the case of nanolaminated samples which by their nature sit above this percolation threshold.

In this work the laminate refractive indices were measured and determined via the replacement of the overall structure of the discrete layers $[n_{\text{IGZO}}/n_{\text{TiO}_2}]_i$ with a singular laminate dielectric function, n_L , which fully describes the action of the superstructure on the incident light. This method is valid as long as all the individual layer thicknesses d are much thinner than the wavelength λ . The validity of the approach in the case of general two-dimensional structures has been demonstrated previously by other researchers [33,34]. In the following we explicitly confirm it for the structures discussed here. To do so, it is vital that the following two criteria are verified:

(i) that constructing a singular dielectric function for the nanolaminate produces an equivalent result to considering the discrete dielectric function and the thickness of each individual layer using full transfer matrix calculations, and

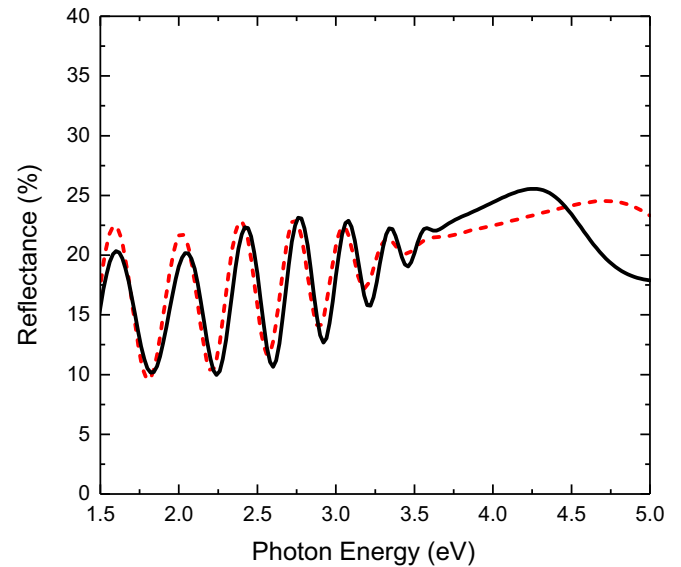


FIG. 4. Comparison of the reflection determined from fitting the dielectric function of a nanolaminate via the laminate dielectric methodology and by using the bulk dielectric functions as input parameters. The reflection of a 600-nm nanolaminate of $[\text{a-IGZO}/\text{TiO}_2]_i$ is calculated via both methods. The nanolaminate used has an a-IGZO layer thickness equal to the TiO₂ layer thickness both for the calculation using the laminate dielectric function and for that using the bulk values. The solid line denotes the laminate dielectric function and the dashed line denotes individual dielectric functions for $[\text{a-IGZO}/\text{TiO}_2]_i$ [7.5 nm/7.5 nm]_i.

(ii) that the nanolaminates discussed in this work fulfill the $\lambda \gg d$ condition, i.e., that the layer thicknesses discussed are sufficiently small for the n_L behavior to hold in the visible range.

To demonstrate criterion (i) the dielectric function of the $[\text{a-IGZO}/\text{TiO}_2]_i$ 10/10 nanolaminate was calculated by two methodologies. The first was the replacement of the stack by a single dielectric function, i.e., the laminate dielectric methodology. The second was the calculation of the dielectric function of the nanolaminate stack by inputting of the dielectric functions and thicknesses of each a-IGZO and TiO₂ layer in a periodic stack manner, which we refer to as the discrete methodology.

For the laminate methodology the reflectance was calculated for a 600-nm-thick nanolaminate, using n_L derived from a $[(\text{a-IGZO})_{10\text{nm}}/(\text{TiO}_2)_{10\text{nm}}]_9$ sample. For the discrete methodology the dielectric function of the stack was constructed from the separate layers with the dielectric functions n_{IGZO} and n_{TiO_2} obtained from measurements of a 110-nm a-IGZO film and a 50-nm TiO₂ film. The total number of layers was chosen such that a similar total thickness of 600 nm was reached, e.g., for 10-nm individual layer thickness the IGZO/TiO₂ bilayer was repeated 30 times. The calculated reflectance spectra are given in Fig. 4. Spectra generated by the laminate and discrete methods are very similar, supporting the validity of the much simpler laminate dielectric function methodology. The small differences observed can be attributed not to the failure of the laminate methodology but rather to the limitations of the discrete approach, which

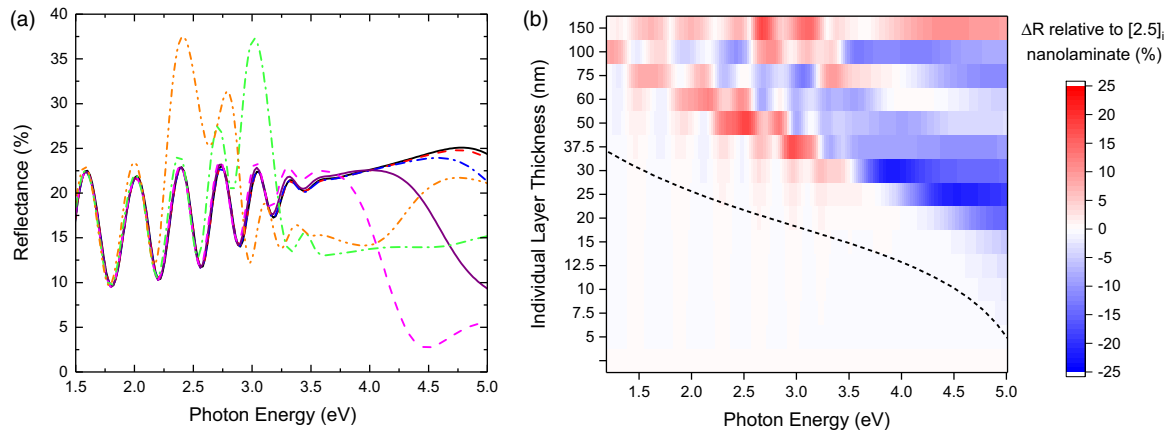


FIG. 5. (a) Calculated reflectance of 600-nm-thick $[a\text{-IGZO}/\text{TiO}_2]_i$ nanolaminates with varying individual layer thicknesses using the discrete methodology. (—) $[2.5/2.5]_{120}$, (---) $[5/5]_{60}$, (-·-) $[12.5/12.5]_{24}$, (—) $[20/20]_{15}$ (---) $[25/25]_{12}$, (-·-) $[37.5/37.5]_8$, and (·-·-) $[50/50]_6$. The overall reflectance in the visible region remains similar up to an individual layer thickness of 20–25 nm, beyond which deviations occur, indicating the breakdown of the $\lambda \gg d$ requirement. (b) Relative change of the reflectance (ΔR) compared to that of a $[2.5/2.5]_i$ $[a\text{-IGZO}/\text{TiO}_2]_i$ superlattice ($\Delta R_{Y-2.5}$). The dashed line approximates the energy at which an $\approx 0.5\%$ reflectance change is observed. In the color graph a positive ΔR is shown in red while a negative is indicated in blue.

must make the assumption that the measured bulklike n_{IGZO} and n_{TiO_2} remain unchanged in the 10-nm layers within the multilayer. In reality such films will exhibit small deviations due to size and confinement effects, deposition conditions, or effects of the layering itself. In particular differences around 1.5–2.5 eV are caused by the defect absorption in ultrathin TiO_2 which are not observed to the same extent in thicker TiO_2 reference films. As a result we conclude that the use of a laminate dielectric function is not only valid but is actually beneficial in determining an accurate dielectric function and hence optical constants as long as the $\lambda \gg d$ requirement is fulfilled.

To confirm the latter, criteria (ii) must be verified for the spectral regions considered here. To do so the reflectances of a set of $[a\text{-IGZO}/\text{TiO}_2]_i$ nanolaminates with varying individual layer thicknesses were calculated and compared. In each of these calculations the overall thickness of the nanolaminates was kept constant at 600 nm and the a-IGZO layer thickness was kept equal to the TiO_2 layer thickness for all calculations (e.g., the volume fraction was kept constant). As a result of the consistent overall thickness, variations in the calculated optical response of the nanolaminates only relate to the change in the individual layer thickness. The initial and terminating layer of each nanolaminate was kept consistent for each sample. Calculations were performed for nanolaminates of 2.5-, 5-, 7.5-, 10-, 12.5-, 15-, 20-, 25-, 37.5-, 50-, and 100-nm individual layer thicknesses.

The results are plotted in Fig. 5. It is observed that the reflectance of the nanolaminate is effectively unchanged in the 1–4 eV range from individual layer thickness of 2.5 nm up to 25 nm, where the reflectance begins to diverge above 3 eV. In order to understand the point of breakdown of the integral reflectance behavior it is beneficial to look at the nanolaminates in terms of variation of reflectivity. This is highlighted in Fig. 5(b), which depicts the change in reflectance of a set of nanolaminates of various thicknesses relative to one of $[2.5 \text{ nm}]_i$ layer thickness. White indicates that the reflectance is close to unchanged ($<1\%$ variation),

whereas red and blue indicate an increase or decrease, respectively, of the reflectance at that energy. It can be observed that the reflectance of the nanolaminates in the visible range is effectively unchanged from $[2.5/2.5]_i$ to $[20/20]_i$. The dashed line indicates the approximate thicknesses at which the $\lambda \gg d$ fails for a given energy. From this we can observe that the $[a\text{-IGZO}/\text{TiO}_2]_i$ nanolaminates will exhibit an integral n_L so long as the individual thickness of the layers remains below 20 nm. This demonstrates that all nanolaminates examined here can be accurately described by an integral n_L in the visible range, and also that the concept of an integral n_L is an effective way to treat the effective index of high-periodicity multilayers as expected. Indeed previous attempts to describe the optical response of $[\text{TiO}_2/\text{Al}_2\text{O}_3]_i$ by fitting each individual layer thickness (discrete methodology) gave inconsistent results with respect to measured layer thickness by transmission electron microscopy [51]. This is understood as our simulation shows that only the volume fraction of the two materials is of relevance in the ultrathin regime, and hence treating each layer individually results in a mathematically overdefined system with unreliable results.

It is important to note that the above calculations assume normal incidence of the light, with the electric field vectors being in plane. The anisotropic nature of the refractive index of the nanolaminate means that some variation in the optical response could be observed for different angles of incidence. These variations would manifest primarily in a change of the apparent thickness of the individual layers at differing angles. This could lead to a breakdown of the $\lambda \gg d$ requirement at lower values of thickness than those obtained here. Unfortunately while we expect the effect to be small in the nanolaminates discussed here, due to limitations in our simulation software we are unable to describe an anisotropic n_L . Fortunately a first approximation of the effect on the angular dependent thickness can be performed using a simple geometric consideration of the problem. The primary expected effect of the angular dependence is to increase the light's path length in the individual layers, leading to a

breakdown of the $\lambda \gg d$ criteria already for thinner films. This simply means that the maximum incidence angle at which any TCO-containing device must function should be considered in the planning stage so that an appropriate nanolaminate periodicity can be selected.

III. CONCLUSION

We have demonstrated a technique to tune the refractive index of a-IGZO by creating an $[a\text{-IGZO}/\text{TiO}_2]_i$ nanolaminate which maintains a-IGZO's original electrical properties. The refractive index of a-IGZO was successfully increased in a controlled way from 2 to 2.4. The conductivity of the overall superstructure was maintained at over 70% of its original value. This high mobility retention is attributed to the alignment of the conduction band of a-IGZO and TiO_2 , which presents a low barrier to transport and allows for carrier exchange between individual layers. This illustrates the potential of nanolaminates for synthesis of laminate TCOs with tuned optical properties and demonstrates that significant

enhancement can be obtained by consideration of the TCOs and dielectric band structure. By careful selection of materials this method can be expanded to other TCOs, reducing internal reflections at interfaces between materials of high refractive index offset such as often happens in devices such as solar cells. We have also demonstrated the applicability of the laminate medium model to the high-periodicity nanolaminates here and have calculated that the laminate dielectric function behavior in the visible range will fail when the individual layer thickness is increased beyond 20 nm, where full multilayer models would be required.

ACKNOWLEDGMENTS

This publication has emanated from research conducted with the financial support of Science Foundation Ireland (SFI) under Grants No. SFI/12/RC/2278 and No. 12/IA/1264. This work was also supported by the Higher Education Authority under the PRTL scheme, cycle 5, and the Irish Research Council under Grant No. GOI/PG/2013/445.

-
- [1] U. Betz, M. K. Olsson, J. Marthy, M. Escolá, and F. Atamny, *Surf. Coat. Technol.* **200**, 5751 (2006).
- [2] H. Yabuta, M. Sano, K. Abe, T. Aiba, T. Den, H. Kumomi, K. Nomura, T. Kamiya, and H. Hosono, *Appl. Phys. Lett.* **89**, 112123 (2006).
- [3] K. Nomura, H. Ohta, A. Takagi, T. Kamiya, M. Hirano, and H. Hosono, *Nature (London)* **432**, 488 (2004).
- [4] C. Granqvist, *Sol. Energy Mater. Sol. Cells* **91**, 1529 (2007).
- [5] K. L. Chopra, P. D. Paulson, and V. Dutta, *Prog. Photovoltaics* **12**, 69 (2004).
- [6] R. L. Hoye, K. P. Musselman, and J. L. MacManus-Driscoll, *APL Mater.* **1**, 060701 (2013).
- [7] K. Ellmer and A. Bikowski, *J. Phys. D: Appl. Phys.* **49**, 413002 (2016).
- [8] G. Gu, V. Bulović, P. Burrows, S. Forrest, and M. Thompson, *Appl. Phys. Lett.* **68**, 2606 (1996).
- [9] R.-P. Xu, Y.-Q. Li, and J.-X. Tang, *J. Mater. Chem. C* **4**, 9116 (2016).
- [10] M. Born and E. Wolf, *Principles of Optics*, 7th ed. (Cambridge University, Cambridge, England, 2002).
- [11] M. Kursawe, R. Anselmann, V. Hilarius, and G. Pfaff, *J. Sol-Gel Sci. Technol.* **33**, 71 (2005).
- [12] S. Ghosh, A. Sarkar, S. Chaudhuri, and A. Pal, *Vacuum* **42**, 645 (1991).
- [13] R. Synowicki, *Thin Solid Films* **313–314**, 394 (1998).
- [14] C. Talagrand, X. Boddart, D. Selmeczi, C. Defranoux, and P. Collot, *Thin Solid Films* **590**, 134 (2015).
- [15] M. Berginski, J. Hüpkes, M. Schulte, G. Schöpe, H. Stiebig, B. Rech, and M. Wuttig, *J. Appl. Phys.* **101**, 074903 (2007).
- [16] K. Fleischer, E. Arca, C. Smith, and I. Shvets, *Appl. Phys. Lett.* **101**, 121918 (2012).
- [17] B. R. K. Nanda, S. Satpathy, and M. S. Springborg, *Phys. Rev. Lett.* **98**, 216804 (2007).
- [18] K. Matsumoto, M. Haruta, M. Kawai, A. Sakaiguchi, N. Ichikawa, H. Kurata, and Y. Shimakawa, *Sci. Rep.* **1**, 27 (2011).
- [19] C.-Y. Wang, C. Fuentes-Hernandez, M. Yun, A. Singh, A. Dindar, S. Choi, S. Graham, and B. Kippelen, *ACS Appl. Mater. Interfaces* **8**, 29872 (2016).
- [20] L. H. Kim, K. Kim, S. Park, Y. J. Jeong, H. Kim, D. S. Chung, S. H. Kim, and C. E. Park, *ACS Appl. Mater. Interfaces* **6**, 6731 (2014).
- [21] W. Choi, S. Lee, J. You, S. Lee, and H. Lee, *Nat. Commun.* **6**, 7424 (2015).
- [22] J. Chakhalian, J. Freeland, G. Srajer, J. Stremper, G. Khaliullin, J. Cezar, T. Charlton, R. Dalgliesh, C. Bernhard, G. Cristiani, H. U. Habermeier, and B. Keimer, *Nat. Phys.* **2**, 244 (2006).
- [23] Y. Baek, S. Lim, L. H. Kim, S. Park, S. W. Lee, T. H. Oh, S. H. Kim, and C. E. Park, *Org. Electron.* **28**, 139 (2016).
- [24] I. Iatsunskiy, E. Coy, R. Viter, G. Nowaczyk, M. Jancelewicz, I. Baleviciute, K. Załeski, and S. Jurga, *J. Phys. Chem. C* **119**, 20591 (2015).
- [25] R. Viter, I. Iatsunskiy, V. Fedorenko, S. Tumenas, Z. Balevicius, A. Ramanavicius, S. Balme, M. Kempniński, G. Nowaczyk, S. Jurga, and M. Bechelany, *J. Phys. Chem. C* **120**, 5124 (2016).
- [26] A. A. Chaaya, R. Viter, I. Baleviciute, M. Bechelany, A. Ramanavicius, Z. Gertner, D. Ert, V. Smyntyna, and P. Miele, *J. Phys. Chem. C* **118**, 3811 (2014).
- [27] M. Lorenz, G. Wagner, V. Lazenka, P. Schwinkendorf, H. Modarresi, M. Van Bael, A. Vantomme, K. Temst, O. Oeckler, and M. Grundmann, *Appl. Phys. Lett.* **106**, 012905 (2015).
- [28] R. Venkatasubramanian, E. Siivola, T. Colpitts, and B. O'Quinn, *Nature (London)* **413**, 597 (2001).
- [29] H. Ohta, *Phys. Status Solidi B* **245**, 2363 (2008).
- [30] J. M. O. Zide, D. Vashaee, Z. X. Bian, G. Zeng, J. E. Bowers, A. Shakouri, and A. C. Gossard, *Phys. Rev. B* **74**, 205335 (2006).
- [31] G. Bulman, P. Barletta, J. Lewis, N. Baldasaro, M. Manno, A. Bar-Cohen, and B. Yang, *Nat. Commun.* **7**, 10302 (2016).
- [32] D. Caffrey, E. Norton, C. Ó. Coileáin, C. M. Smith, B. Bulfin, L. Farrell, I. V. Shvets, and K. Fleischer, *Sci. Rep.* **6**, 33006 (2016).

- [33] W. Plieth and K. Naegle, *Surf. Sci.* **64**, 484 (1977).
- [34] O. Hunderi and K. Johannessen, *Superlattices Microstruct.* **3**, 193 (1987).
- [35] S. Boukrouh, R. Bensaha, S. Bourgeois, E. Finot, and M. M. de Lucas, *Thin Solid Films* **516**, 6353 (2008).
- [36] H. Tang, K. Prasad, R. Sanjines, P. E. Schmid, and F. Levy, *J. Appl. Phys.* **75**, 2042 (1994).
- [37] T. Luttrell, S. Halpegamage, J. Tao, A. Kramer, E. Sutter, and M. Batzill, *Sci. Rep.* **4**, 4043 (2014).
- [38] See Supplemental Material at <http://link.aps.org/supplemental/10.1103/PhysRevMaterials.2.096002> for further information on the x-ray reflectivity measurements, TiO₂ stoichiometry, and valence band offset measurements.
- [39] J. Banfield and D. Veblen, *Am. Mineral.* **77**, 545 (1992).
- [40] B. Prasai, B. Cai, M. Underwood, J. Lewis, and D. Drabold, *J. Mater. Sci.* **47**, 7515 (2012).
- [41] T. A. König, P. A. Ledin, J. Kerszulis, M. A. Mahmoud, M. A. El-Sayed, J. R. Reynolds, and V. V. Tsukruk, *ACS Nano* **8**, 6182 (2014).
- [42] J. M. Ball, S. D. Stranks, M. T. Hörantner, S. Hüttner, W. Zhang, E. J. Crossland, I. Ramirez, M. Riede, M. B. Johnston, and R. H. Friend, *Energy Environ. Sci.* **8**, 602 (2015).
- [43] A. Galca, G. Socol, and V. Craciun, *Thin Solid Films* **520**, 4722 (2012).
- [44] H.-H. Hsu, C.-Y. Chang, C.-H. Cheng, S.-H. Chiou, and C.-H. Huang, *IEEE Electron Device Lett.* **35**, 87 (2014).
- [45] K. Lee, K. Nomura, H. Yanagi, T. Kamiya, E. Ikenaga, T. Sugiyama, K. Kobayashi, and H. Hosono, *J. Appl. Phys.* **112**, 033713 (2012).
- [46] J. Robertson, *J. Non-Cryst. Solids* **303**, 94 (2002).
- [47] S. Valencia, J. Marin, and G. Restrepo, *Open Mater. Sci. J.* **4**, 9 (2010).
- [48] D. O. Scanlon, C. W. Dunnill, J. Buckeridge, S. A. Shevlin, A. J. Logsdail, S. M. Woodley, C. R. A. Catlow, M. J. Powell, R. G. Palgrave, I. P. Parkin, G. W. Watson, T. W. Keal, P. Sherwood, A. Walsh, and A. A. Sokol, *Nat. Mater.* **12**, 798 (2013).
- [49] J. C. M. Garnett, *Philos. Trans. R. Soc. A* **205**, 237 (1906).
- [50] D. Bruggeman, *Ann. Phys.* **416**, 665 (1935).
- [51] D. R. Mitchell, D. Attard, K. Finnie, G. Triani, C. Barbé, C. Depagne, and J. Bartlett, *Appl. Surf. Sci.* **243**, 265 (2005).